Inorganics **2014**, *2*, 233-247; doi:10.3390/inorganics2020233

OPEN ACCESS

inorganics

ISSN 2304-6740

www.mdpi.com/journal/inorganics

Article

Supercritical Fluid Synthesis of $LiCoPO_4$ Nanoparticles and Their Application to Lithium Ion Battery

Murukanahally Kempaiah Devaraju *, Quang Duc Truong, Hiroshi Hyodo, Takaaki Tomai and Itaru Honma *

Institute of Multidisciplinary Research for Advanced Materials, Tohoku University, 2-1-1, Katahira, Aoba-ku, Sendai 980-8577, Japan; E-Mails: tqduc@mail.tagen.tohoku.ac.jp (Q.D.T.); hyodo@tagen.tohoku.ac.jp (H.H.); tomai@tagen.tohoku.ac.jp (T.T.)

* Authors to whom correspondence should be addressed;
E-Mails: devaraju113@gmail.com (M.K.D.); i.honma@tagen.tohoku.ac.jp (I.H.);
Tel.: +81-22-217-5816 (I.H.); Fax: +81-22-217-5828 (I.H.).

Received: 31 October 2013; in revised form: 23 January 2014 / Accepted: 19 May 2014 / Published: 28 May 2014

Abstract: In this work, $LiCoPO_4$ nanoparticles were synthesized by supercritical fluid method using cobalt nitrate hexahydrate ($Co(NO_3)_2$ $6H_2O$) and cobalt acetate tetrahydrate ($C_4H_6CoO_4$ $4H_2O$) as starting materials. The effect of starting materials on particle morphology, size, and the crystalline phase were investigated. The as-synthesized samples were systematically characterized by XRD, TEM, STEM, EDS, BET, and TG and charge-discharge measurements. In addition, Rietveld refinement analysis was performed. The electrochemical measurements of $LiCoPO_4$ nanoparticles have shown differences in capacities depending on the starting materials used in the synthesis and the results have been discussed in this paper.

Keywords: supercritical fluid; starting materials; high voltage; nanoparticles; $LiCoPO_4$ cathode

---

1. Introduction

In recent years, rechargeable lithium ion batteries have received great attention due to their importance in power sources for electric and hybrid electric vehicles and they offer many more opportunities in electric and electronic domain with higher energy densities than the commercially

available rechargeable batteries [1,2]. The crucial factors for the success of new cathode materials depend on the synthesis method, starting materials, particle size, cation order, and other experimental parameters [3]. Since the demonstration of electrochemical properties of $LiFePO_4$ cathode material by Padhi *et al.* [4] olivine-type $LiMPO_4$ (M = Fe, Mn, Co and Ni) and Nasicon-type $Li_3V_2(PO_4)_3$ have received great interest owing to their low cost, high reversible capacity, and good stability [5–8]. The potential of the M^{3+}/M^{2+} redox couple *versus* Li/Li^+ of $LiMPO_4$ is as follows; 3.5 V for $LiFePO_4$, 4.1 V for $LiMnPO_4$, 5.2–5.4 V for $LiNiPO_4$, and 4.8 V for $LiCoPO_4$. Among these, $LiCoPO_4$ is appealing since it offers both a flat high potential (~4.8 V *vs.* Li/Li^+) and good theoretical capacity (167 mA h/g) [9]. The cyclic and rate performances of $LiCoPO_4$ material is affected by electrolyte degradation which is due to high working voltage, low electronic conductivity, and low intrinsic conductivity. Thus far, the first cycle discharge capacities of 30–140 mA h/g with poor or moderate cyclic performances have been observed for $LiCoPO_4$ synthesized via different synthetic routes. In recent days, effort has been made to improve the cyclic performances by cationic doping and decreasing the particle size. Particularly, $LiCoPO_4$ nanoparticles have shown improved electrochemical performances, which is due to a small Li ion diffusion length. In addition, nanoparticles facilitate fast charge and mass transport because of large surface to volume ratio, as well as enhancing the close contact with the electrolyte and which could speed up the reaction kinetics.

$LiCoPO_4$ cathode material can be synthesized by various methods, such as solid-state reaction [10–17], hydrothermal synthesis [18–20], sol–gel method [11,21,22], co-precipitation [23], optical floating zone method [24], radio frequency magnetron sputtering [25], electrostatic spray deposition technique [26], and microwave heating method [27]. In addition, some approaches have been applied in order to improve the electronic conductivity of the cathode, such as carbon coating [11], making composite with carbon [10,28]. However, most of the above methods required long duration time to synthesize $LiCoPO_4$ particles, and often it is not easy to control the shape and size of the synthesized particles. Among these methods, hydrothermal and solvothermal process have proved to be beneficial in terms of cost, time and energy savings [29,30]. Very recently, we reported supercritical fluid process for controlled synthesis of plate-like $LiCoPO_4$ nanoparticles within a short reaction time [31]. Supercritical fluid method possess unique properties, such as gas like diffusivity, low viscosity, and the density of the reactants closer to that of liquid, these properties leads to the preparation of high quality materials. In recent days, varieties of electrode materials have been successfully synthesized via supercritical fluid process [32–38]. Recently, our group has reported supercritical fluid synthesis of nanosize lithium metal phosphates [30,38,39], lithium metal silicates [40–44], and flurophosphates [45].

Herein, we report supercritical fluid synthesis of $LiCoPO_4$ nanoparticles using two kinds of starting materials, such as cobalt nitrate hexahydrate ($Co(NO_3)_2$ $6H_2O$) and cobalt acetate tetrahydrate ($C_4H_6CoO_4$ $4H_2O$). The reaction was carried out at 400 °C within a short reaction period (7 min). The effect of starting materials on the crystalline structure and particles size were investigated and their electrochemical properties have been characterized.

2. Results and Discussion

2.1. One Pot Synthesis

Supercritical fluid process is a one pot synthesis process for $LiCoPO_4$ nanoparticles as shown in Figure 1. Two kinds of precursor solution were used for the synthesis of $LiCoPO_4$ nanoparticles. For the synthesis, 5 ml of precursor solution was fed into the supercritical reactor and heated at 400 °C for 7 min to obtain well-crystallized $LiCoPO_4$ nanoparticles.

Figure 1. One pot synthesis of $LiCoPO_4$ nanoparticles using two kinds of starting materials via supercritical fluid process.

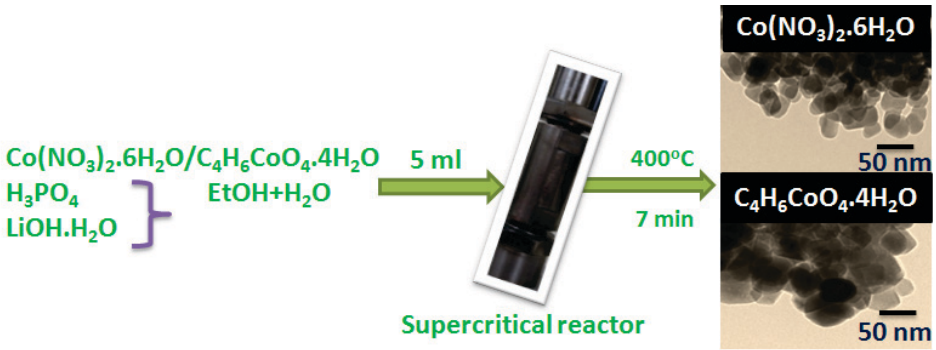

2.2. X-ray Powder Diffraction Analysis

The XRD patterns of as-synthesized $LiCoPO_4$ particles at 400 °C for 7 min using $Co(NO_3)_2$ $6H_2O$ and $C_4H_6CoO_4$ $4H_2O$ as starting materials via supercritical fluid process are shown in Figure 2.

Figure 2. XRD patterns of $LiCoPO_4$ nanoparticles synthesized using (**a**) $Co(NO_3)_2$ $6H_2O$ and (**b**) $C_4H_6CoO_4$ $4H_2O$ via supercritical fluid process; (**c**) crystal structure of $LiCoPO_4$.

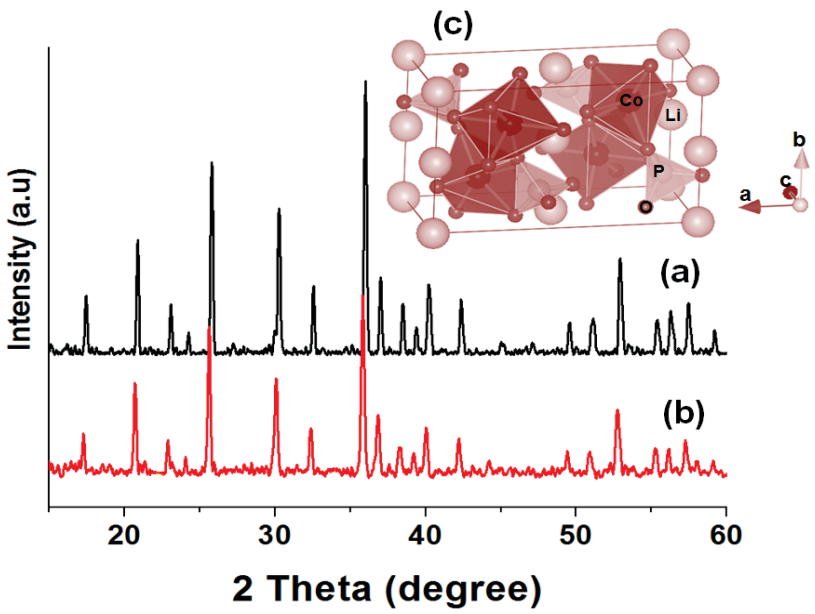

The observed diffraction peaks of both $LiCoPO_4$ particles are well matched with JCPDS file (# 00-085-0002), and belongs to orthorhombic crystal system with *Pnma* space group. The XRD patterns are in agreement with the reported pattern [23,31,46–49]. The calculated cell parameters and the Rietveld reliability factors for $LiCoPO_4$ particles synthesized using $Co(NO_3)_2$ $6H_2O$ and $C_4H_6CoO_4$ $4H_2O$ are a = 10.222Å, b = 5.9273, c = 4.7088, R_{WP} = 29.42%, R_I = 13.19% and a = 10.2046Å, b = 5.9183, c = 4.6977, R_{WP} = 27.63%, R_I = 16.22%, respectively. The cell parameters are almost consistent with the reported values [50–52]. The Rietveld refinement results obtained from XRD pattern are shown in Table 1, the results showed almost same structural parameters for $LiCoPO_4$ nanoparticles synthesized using $Co(NO_3)_2$ $6H_2O$ and $C_4H_6CoO_4$ $4H_2O$. The experimental, calculated and observed XRD pattern are shown in Figure S1(a,b) (Supplementary information), which show no significant changes and impurity phases. From the XRD results, it is confirmed that single phase of $LiCoPO_4$ was synthesized using $Co(NO_3)_2$ $6H_2O$ (Figure 1(a)) and $C_4H_6CoO_4$ $4H_2O$ (Figure 1(b)) as starting materials via supercritical fluid process. The XRD pattern did not shows much difference except variations in the peak intensity. Due to higher solubility of $Co(NO_3)_2$ $6H_2O$ in water-ethanol, the particles are well crystallized, so that the peak intensity of $LiCoPO_4$ particles synthesized using $Co(NO_3)_2$ $6H_2O$ is higher than that of $LiCoPO_4$ particles synthesized using $C_4H_6CoO_4$ $4H_2O$. The model of $LiCoPO_4$ crystal structure is shown in Figure 2(c), which shows the arrangement of cobalt octahedral and phosphor tetrahedral linked with oxygen either by corner sharing or edge sharing. It is also proved that, regardless of using different source materials in the present synthesis, supercritical fluid process is capable of producing high quality $LiCoPO_4$ nanoparticles.

Table 1. Rietveld refinement results of XRD pattern of $LiCoPO_4$ synthesized using $Co(NO_3)_2$ $6H_2O$ and $C_4H_6CoO_4$ $4H_2O$.

Formula Crystal system Space group		**$LiCoPO_4$ (Using $Co(NO_3)_2$ $6H_2O$) Orthorhombic *Pnma***					**$LiCoPO_4$ (Using $C_4H_6CoO_4$ $4H_2O$) Orthorhombic *Pnma***				
Atom	**Site**	**X**	**Y**	**Z**	**g**	**B/Å^2**	**X**	**Y**	**Z**	**g**	**B/Å^2**
Li	4a	0.5	0.5	0.5	1	0.8	0.5	0.5	0.5	1	0.8
Co	4c	0.2778	0.25	0.9819	1	1.0	0.2783	0.25	0.9801	1	1.0
P	4c	0.096	0.25	0.420	1	1.5	0.096	0.25	0.416	1	1.5
O(1)	4c	0.091	0.25	0.736	1	1.7	0.085	0.25	0.728	1	1.7
O(2)	4c	0.453	0.25	0.240	1	0.6	0.445	0.25	0.230	1	0.6
O(3)	8d	0.160	0.029	0.278	1	0.9	0.157	0.0276	0.275	1	0.9

2.3. TEM and HRTEM Analysis

The as-synthesized particles morphology, size and their crystalline nature are observed by TEM and HRTEM analysis and the results are shown in Figure 3(a–d) and Figure 3(e–h). The particles synthesized at 400 °C for 7 min using $Co(NO_3)_2$ $6H_2O$ (Figure 3(a–d)) and $C_4H_6CoO_4$ $4H_2O$ (Figure 3(e–h)) as starting materials via supercritical fluid process show mixed type morphologies, such as sphere, plate, and rod. The particles size are ranging from 20–50 nm in diameter for as-synthesized $LiCoPO_4$ particles using $Co(NO_3)_2$ $6H_2O$ (Figure 3(a,b)) and $C_4H_6CoO_4$ $4H_2O$ (Figure 3(e,f)) as starting materials. The as-synthesized particles are well distributed and softly agglomerated. The ED

pattern and HRTEM images of as-synthesized particles using $Co(NO_3)_2$ $6H_2O$ and $C_4H_6CoO_4$ $4H_2O$ are shown in Figure 3(c,d) and Figure 3(g,h), respectively. The SAED images of both samples (Figure 3(c,g)) are exhibited dot like pattern, which clearly shows the single crystalline nature of $LiCoPO_4$ particles. However, as-synthesized particles using $Co(NO_3)_2$ $6H_2O$ (Figure 4(c)) show weaker diffraction than the SAED pattern of as-synthesized particle using $C_4H_6CoO_4$ $4H_2O$ (Figure 3(g)). The HRTEM images show well resolved lattice fringes exhibiting interplanar spacing along [001] and [100] axis as shown in Figure 3(d,h). The interplanar spacing along *a* axis show 1.02 nm which is consistent with the unit cell parameter of olivine structured $LiCoPO_4$ along *a*-axis (a = 10.02 A°). $LiCoPO_4$ nanoparticles synthesized using two kinds of starting materials within a short reaction time via supercritical fluid process show well crystalline nanosize particles. In order to investigate effect of temperature and time on the particles formation, synthesis was carried out using $Co(NO_3)_2$ $6H_2O$ and $C_4H_6CoO_4$ $4H_2O$ as starting materials and the results are shown in Table 2. When the reaction temperature was 300 °C, sphere like particles were observed at 7, 10, and 15 min of reaction time with particles size ranging from 10–30 nm, the XRD pattern of this particles show nearly amorphous phase and particles were covered with lot of carbonaceous materials. When the reaction temperature was increased to 350 °C for about 7, 10, and 15 min of reaction time, the obtained particles were sphere and rod like particles with 20–70 nm in diameter. The XRD of these particles show mixed phase of $LiCoPO_4$, and Li_3PO_4 phase. Single phase $LiCoPO_4$ particles were obtained only at 400 °C for about 7, 10, and 15 min of reaction time, which were the optimum experimental conditions for the formation of $LiCoPO_4$ under supercritical fluid conditions.

Figure 3. TEM, HRTEM, SAED images of $LiCoPO_4$ nanoparticles synthesized using (**a**–**d**) $Co(NO_3)_2$ $6H_2O$ and (**e**–**h**)$C_4H_6CoO_4$ $4H_2O$ as starting materials.

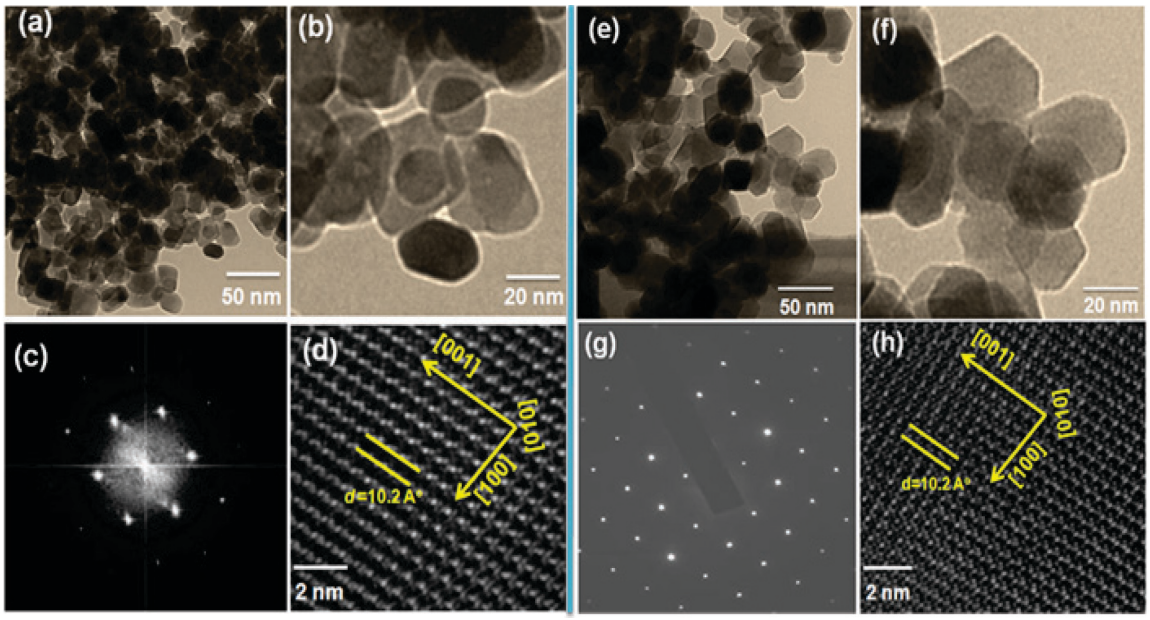

Table 2. Synthesis conditions for $LiCoPO_4$ particles using $Co(NO_3)_2$ $6H_2O$ and $C_4H_6CoO_4$ $4H_2O$ as starting materials.

Synthesis Temperature (°C)	Reaction Time (min)	Morphology	Particle size (nm)	XRD
300	7,10 &15	Sphere	10-30	nearly amorphous
350	7,10 &15	Sphere & rods	10-30	$LiCoPO_4$, Li_3PO_4
400	7,10 &15	Sphere, plates & rods	10-30	$LiCoPO_4$

2.4. Elemental Mapping

The as-synthesized particles using $Co(NO_3)_2$ $6H_2O$ and $C_4H_6CoO_4$ $4H_2O$ as starting materials were subjected to STEM analysis to verify the purity of $LiCoPO_4$ nanoparticles. Figure 4 shows the elemental mapping of both the particles.

Figure 4. STEM images of $LiCoPO_4$ nanoparticles synthesized using $Co(NO_3)_2$ $6H_2O$ and $C_4H_6CoO_4$ $4H_2O$ as starting materials.

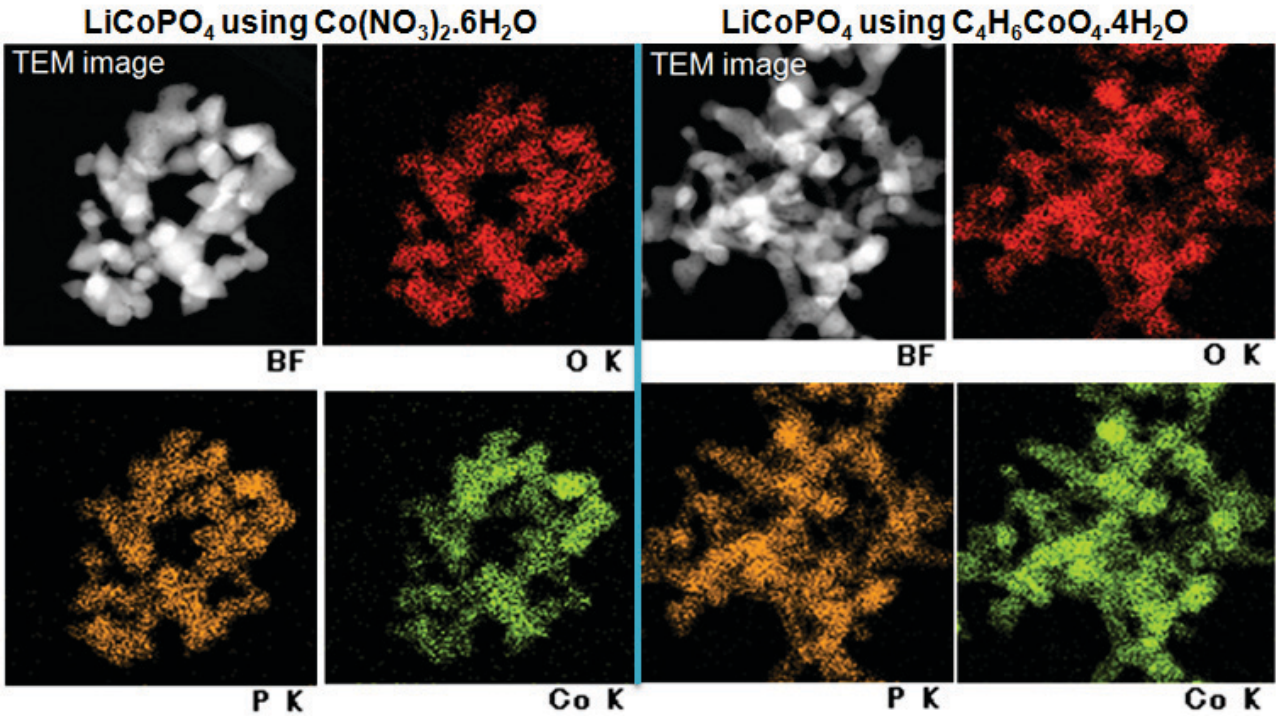

The uniform distribution of oxygen, phosphor and cobalt elements can be clearly observed in the STEM images. This result indicated that the as-synthesized particles have homogeneous elemental distribution and high purity without any impurities. The EDS spectrum of the as-synthesized using $Co(NO_3)_2$ $6H_2O$ and $C_4H_6CoO_4$ $4H_2O$ as starting materials are shown in Figure 5. The particles exhibited characteristic peaks of Co, P, and O elements in $LiCoPO_4$ nanoparticles. The peak below 0.3 eV is corresponds to the carbon peak, the intensity of C peak is higher for the $LiCoPO_4$ nanoparticles synthesized using $C_4H_6CoO_4$ $4H_2O$ as starting material due to the formation of carbon after dissociation reaction of $C_4H_6CoO_4$ $4H_2O$ at supercritical fluid conditions. However, presence of carbon

in these cathode materials is beneficial in order improve the conductivity of the $LiCoPO_4$ nanoparticles during electrochemical reactions [46,47].

Figure 5. EDS of $LiCoPO_4$ nanoparticles synthesized using (**a**) $Co(NO_3)_2$ $6H_2O$ and (**b**) $C_4H_6CoO_4$ $4H_2O$ as starting materials.

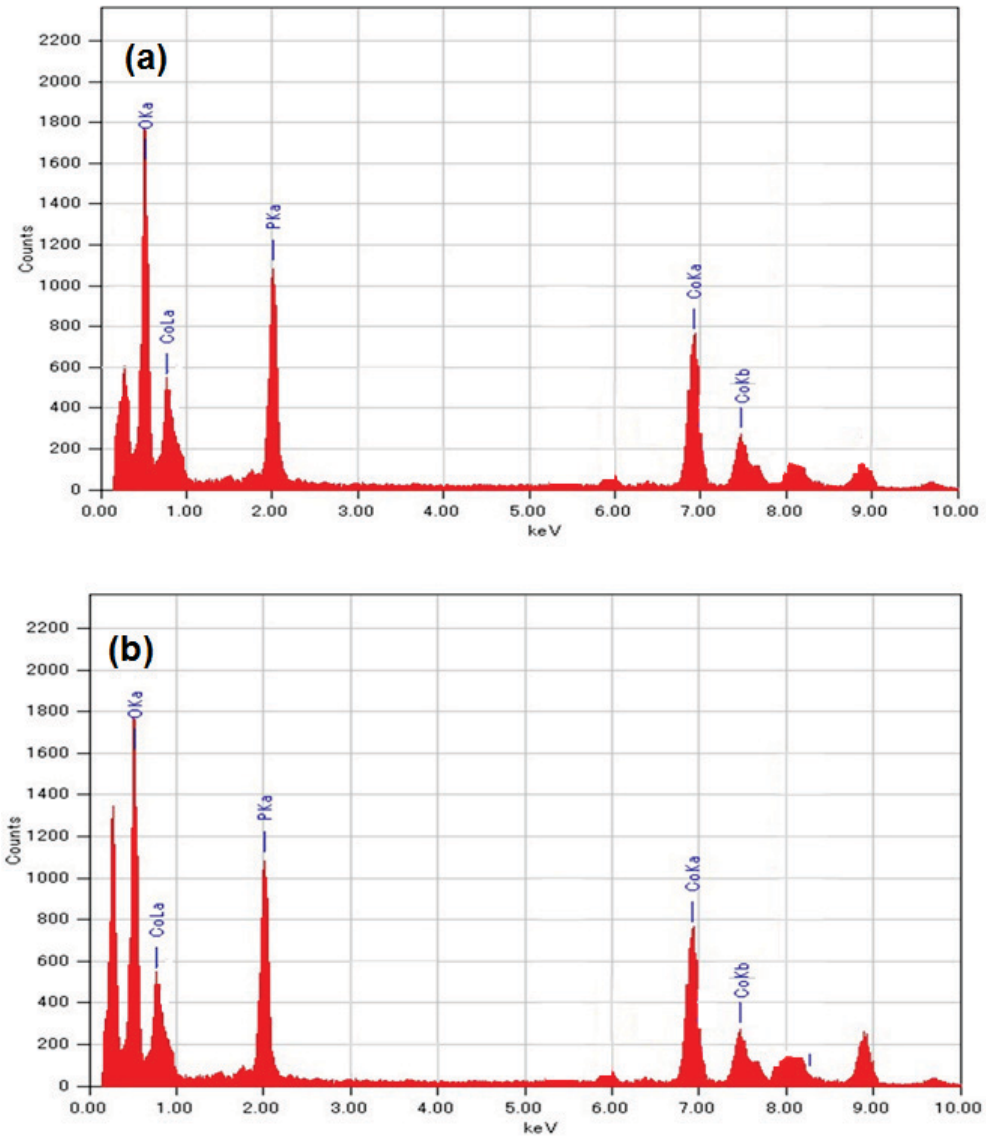

2.5. BET and TG-Analysis

The surface area of the as-synthesized particles using $Co(NO_3)_2$ $6H_2O$ and $C_4H_6CoO_4$ $4H_2O$ are analysed by BET analysis. The surface area of 14.3 m^2/g for $LiCoPO_4$ nanoparticles synthesized using $Co(NO_3)_2$ $6H_2O$ and 16.5 m^2/g for $LiCoPO_4$ particles synthesized using $C_4H_6CoO_4$ $4H_2O$ were observed. Generally, nanosize particles with higher surface area are beneficial for enhanced electrochemical reactions.

The carbon content in the as-synthesized $LiCoPO_4$ nanoparticles using $Co(NO_3)_2$ $6H_2O$ and $C_4H_6CoO_4$ $4H_2O$ are analyzed by TG analysis. The weight loss of 16 wt% for $LiCoPO_4$ nanoparticles synthesized using $Co(NO_3)_2$ $6H_2O$ and 18 wt% for $LiCoPO_4$ particles synthesized using $C_4H_6CoO_4$ $4H_2O$ were

observed as show in Figure 6. The observed weight loss is the weight of carbon present in the as-synthesized particles. This carbon could be amorphous material and is not conductive, which is not useful in improving the electronic conductivity of $LiCoPO_4$ electrode materials.

Figure 6. TG analysis of $LiCoPO_4$ nanoparticles synthesized using (**a**) $Co(NO_3)_2$ $6H_2O$ and (**b**) $C_4H_6CoO_4$ $4H_2O$ as starting materials.

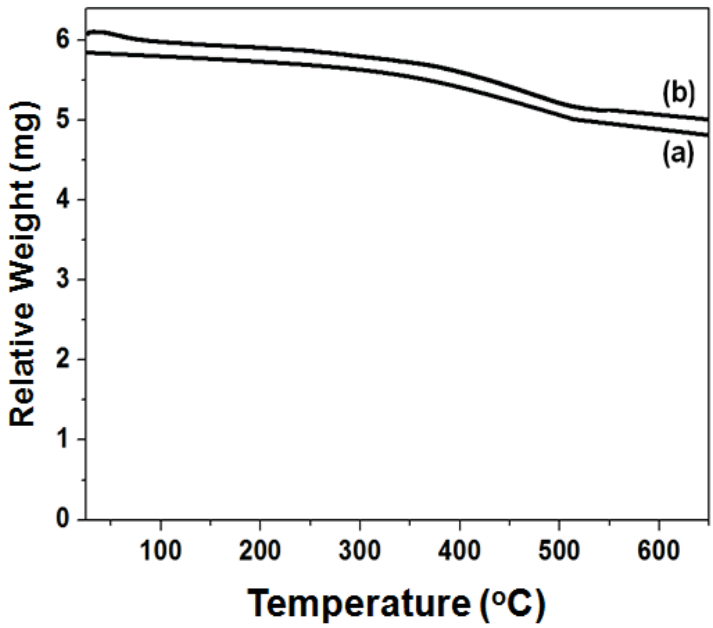

2.6. Electrochemical Performance

The electrochemical performances of as-synthesized particles using $Co(NO_3)_2$ $6H_2O$ and $C_4H_6CoO_4$ $4H_2O$ were measured by galvanostatic charge-discharge method. Figure 7 shows the discharge profiles and cyclic performance (Figure 7(c)) of $LiCoPO_4$ nanoparticles synthesized using $Co(NO_3)_2$ $6H_2O$ (Figure 7(a)) and $C_4H_6CoO_4$ $4H_2O$ (Figure 7 (b)) at 400 °C for 7 min via supercritical fluid process. The discharge measurement was carried out at 0.1C rate for $LiCoPO_4$ nanoparticles, which show a flat discharge curve around 4.75 V. The charge capacities of 150 and 165 $mAhg^{-1}$ for first and second cycle was observed for $LiCoPO_4$ nanoparticles synthesized using $Co(NO_3)_2$ $6H_2O$ as starting material. The charge capacities of 140 mA h g^{-1} and 152 mA h g^{-1} for the first and second cycle were observed for $LiCoPO_4$ nanoparticles, which were synthesized using $C_4H_6CoO_4$ $4H_2O$ as starting material. The discharge capacities of 98 mA h g^{-1} and 115 mA h g^{-1} (Figure 7 (a)) for the first cycle and 62 mA h g^{-1} and 101 mA h g^{-1} (Figure 7(b)) for the second cycles were observed. The origin of discharge capacity of 20 mA h g^{-1} around 2.5–3 V with slope like profile is might be due to the effect of particle size because of high surface area than the bulk particles, which could be responsible for secondary reactions. However, the observed discharge capacities are reasonable and even higher than that of few recently reported discharge capacities of $LiCoPO_4$ particles synthesized by different routes [20,22].

Figure 7. Discharge profiles of $LiCoPO_4$ nanoparticles synthesized using (**a**) $Co(NO_3)_2$ $6H_2O$ and (**b**) $C_4H_6CoO_4$ $4H_2O$ as starting materials; (**c**) cyclic performance.

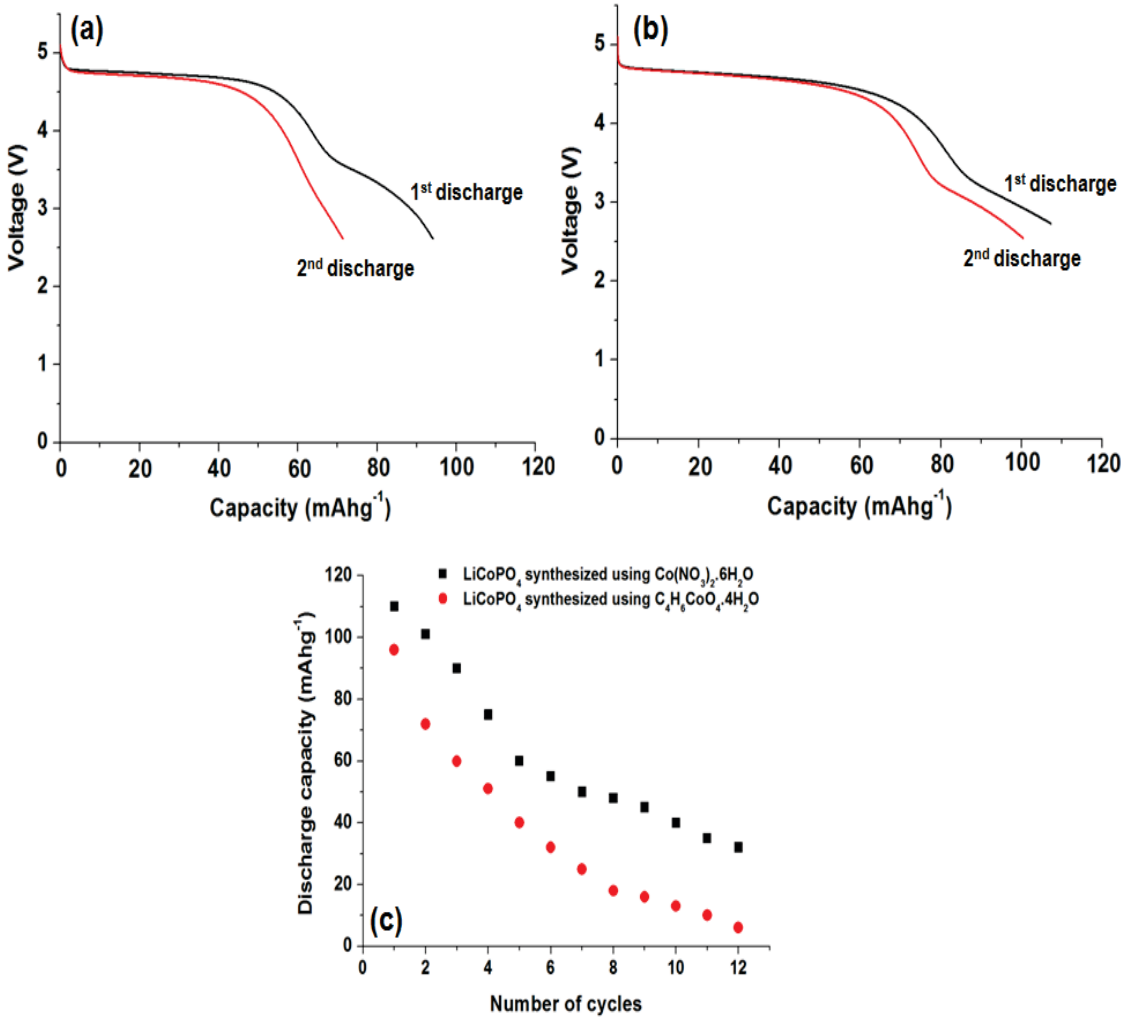

$LiCoPO_4$ nanoparticles synthesized using $C_4H_6CoO_4$ $4H_2O$ show the highest discharge capacities, which might be due to the presence of carbon residue derived from decomposition of $C_4H_6CoO_4$ $4H_2O$ at the supercritical fluid reaction. Probably, this carbon was coated onto the surface of $LiCoPO_4$ nanoparticles, which results in better electronic mobility. However, reasonable discharge capacities observed for both the $LiCoPO_4$ nanoparticles, which are due to the small particle size, good crystallinity, and due to the nature of starting materials used in the synthesis. However, poor cyclic performance was observed for $LiCoPO_4$ nanoparticles (Figure 7 (c)), which is mainly due to the instability of electrolyte at 5 V, and due to the side reactions between electrolyte and electrode and results in the formation a solid-electrolyte interface (SEI) which cause the electrolyte oxidation and lithium loss [47]. Usually, $LiCoPO_4$ cathodes suffered from poor cycling stability [49]. Another possible reason may be due to the antisite defects, where Li^+ site is occupied by Co atom upon charge process and which block the Li^+ during discharge process, so deficiency of lithium is occurred during electrochemical reaction [48]. Further, characterization is necessary to investigate on antisite defects in olivine structured cathode materials, for that ADF/ABF analysis might be very useful to locate the cobalt atoms in lithium site.

3. Experimental Section

3.1. Synthesis of $LiCoPO_4$ Nanoparticles

$LiCoPO_4$ nanoparticles were synthesized using two kinds of starting materials such as cobalt (II) nitrate hexahydrate ($Co(NO_3)_2$ $6H_2O$) and cobalt (II) acetate tetra hydrate ($C_4H_6CoO_4$ $4H_2O$). In a typical synthesis, cobalt (II) nitrate hexahydrate or cobalt (II) acetate tetra hydrate (Wako, Japan), orthophosphoric acid (o-H_3PO_4: Wako, Japan) and lithium hydroxide monohydrate (LiOH H_2O: Wako, Japan) were used in 1:1:1 molar ratio. Ascorbic acid (Wako, Japan) was used as reducing agent. The above starting materials were dissolved in mixed solvents of water and ethanol (1:1 volume ratio), the solution was stirred for 15–20 min and then 0.5 g of ascorbic acid was added to the solution. Later, the solution mixture (5 mL) was transferred to batch reactors (4 reactors, each 10 mL volume) followed by heating at 400 °C for 7 min, then reactors were quenched in cold water, the products were recovered through repeated washings using ethanol and water.

3.2. Material Characterization

The crystalline phase of the samples were characterized using powder X-ray diffraction (XRD; Rigaku RINV-2200, 40 kV and 30 mA) with CuKα radiation (λ = 1.5406 Å)The XRD patterns were analyzed by the Rietveld method using the program RIETAN-2000 [53]. The particles morphology, purity and elemental distribution was observed by transmission electron microscopy (JEOL TEM-2100F), elemental mapping and energy dispersive spectroscopy (EDS, JEM-2010F at 200 KeV). Selected area electron diffraction (SAED) and lattice fringes observation done by using high-resolution transmission electron microscopy (HRTEM, JEOL JEM 2100F, 200 kV). The surface area was measured using a Brunauer–Emmet–Teller (BET, NOVA 4200e) surface area and pore size analyzer. Thermo-gravimetric (TG) analysis was performed in air using a TG-DTA 2000S system to ascertain the exact carbon content in the $LiCoPO_4$ cathode material; the temperature was limited to 650 °C in order to avoid the oxidation of $LiCoPO_4$.

3.3. Electrochemical Performance

The electrochemical performance of $LiCoPO_4$ was investigated using coin-type cells (CR2032). The working electrodes is composed of 83 wt% $LiCoPO_4$ mixed with 10 wt.% acetylene black and 7 wt.% PTFE (poly(tetrafluoroethylene)) as a binder. The electrode paste was spread uniformly and vacuum dried for 12 h at 160 °C. Later, cathode was punched into circular discs and cut into wafers (7 mm in diameter, 0.025 mm in thickness, 3–5 mg). The tested cell was assembled inside an argon-filled glove box. For electrochemical measurements, the cell is composed of lithium metal counter, reference electrodes and a $LiCoPO_4$ positive electrode. 1 M $LiPF_6$ in a mixed solvent of ethylene carbonate (EC) and dimethyl carbonate (DMC) with 1:1 in volume ratio (Tomiyama Pure Chemical Co., Ltd., Tokyo, Japan) was used as the electrolyte. The galvanostatic charge-discharge cycling was performed between 2.5 and 5.1V *versus* Li^+/Li on multi-channel battery testers (Hokuto Denko, Japan). Current densities and specific capacities were calculated on the basis of the weight of $LiCoPO_4$ cathode used in the electrode.

4. Conclusions

$LiCoPO_4$ nanoparticles were successfully synthesized using cobalt (II) nitrate hexahydrate and cobalt (II) acetate tetrahydrate at 400 °C for 7 min via supercritical fluid process. The as-synthesized particles showed 20–50 nm in diameter with mixed type morphology observed by TEM analysis. The starting materials did not affect much on particles size and morphology of $LiCoPO_4$ particles. The phase purity of as-synthesized particles was confirmed by XRD, Rietveld analysis, STEM, and EDS analysis. Electron diffraction analysis and high-resolution image shows that, the particles are single crystalline and exhibits well-aligned crystal planes without any dislocations or defects. The experimental results show that, supercritical fluid process can synthesize single crystalline $LiCoPO_4$ nanoparticles using different kind of starting materials. Further, application of as-synthesized $LiCoPO_4$ nanoparticles as cathode part to Li-ion battery is tested by galvanostatic charge-discharge methods. $LiCoPO_4$ nanoparticles synthesized using cobalt (II) nitrate hexahydrate and cobalt (II) acetate tetra hydrate show reasonable electrochemical performances. The highest discharge capacity of 115 mA h g^{-1} for the first cycle is observed for the nanoparticles synthesized using cobalt (II) acetate tetrahydrate. However, poor cyclic performance was observed for these nanoparticles, conductive carbon coating and protection of interface would require improving the cyclic performance.

Acknowledgments

One of the authors (Murukanahally Kempaiah Devaraju) would like to acknowledge the financial support by Japan Society for Promotion of Science, Japan for their fellowship to carry out the research work.

Author Contributions

M.K.D. and I.H. conceived and designed this work. The synthesis of the material and characterization was carried out by M.K.D. and the paper was written by M.K.D., H.H performed Rietveld analysis. T.T. and Q.D.T. participated in discussion of the results.

Conflicts of Interest

The authors declare no conflict of interest.

References

1. Ceder, G.; Chiang, Y.M.; Sadoway, D.R.; Aydinol, M.K.; Jang, Y.I.; Huang, B. Identification of cathode materials for lithium batteries guided by first-principles calculations. *Nature* **1998**, *392*, 694–696.
2. Andersson, A.M.; Abraham, D.P.; Haasch, R.; MacLaren, S.; Liu, J.; Amine, K. Surface characterization of electrodes from high power lithium-ion batteries. *J. Electrochem. Soc.* **2002**, *149*, A1358–A1369.

3. Chen, J.; Vacchio, M.J.; Wang, S.; Chernova, N.; Zavalij, P.Y.; Whittingham, M.S. The hydrothermal synthesis and characterization of olivines and related compounds for electrochemical applications. *Solid State Ionics* **2008**, *178*, 1676–1693.
4. Padhi, A.K.; Nanjundaswamy, K.S.; Goodenough, J.B. Phospho-olivines as positive-electrode materials for rechargeable lithium batteries. *J. Electrochem. Soc.* **1997**, *144*, 1188.
5. Yang, H.; Wu, X.L.; Cao, M.H.; Guo, Y.G. Solvothermal synthesis of $LiFePO_4$ hierarchically dumbbell-like microstructures by nanoplate self-assembly and their application as a cathode material in lithium-ion batteries. *J. Phys. Chem. C* **2009**, *113*, 3345–3351.
6. Delacourt, C.; Poizot, P.; Morcrette, M.; Tarascon, J.-M.; Masquelier, C. One-step low-temperature route for the preparation of electrochemically active $LiMnPO_4$ powders. *Chem. Mater.* **2004**, *16*, 93–99.
7. Fisher, C.A.J.; Prieto, V.M.H.; Islam, M.S. Lithium Battery Materials $LiMPO_4$ (M = Mn, Fe, Co, Ni): Insights into Defect Association, Transport Mechanisms and Doping Behavior. *Chem. Mater.* **2008**, *20*, 5907–5915.
8. Ren, M.M.; Zhou, Z.; Gao, X.P.; Peng, W.X.; Wei, J.P. Core−shell $Li_3V_2(PO_4)_3$@C composites as cathode materials for lithium-ion batteries. *J. Phys. Chem. C* **2008**, *112*, 5689–5693.
9. Amine, A.; Yasuda, H.; Yamachi, M. Olivine $LiCoPO_4$ as 4.8 V electrode material for lithium batteries. *Electrochem. Solid-State Lett*. **2000**, *3*, 178.
10. Rabanal, M.E.; Gutierrez, M.C.; Garcia-Alvarado, F.; Gonzalo, E.C.; Arroyo-de Dompablo, M.E. Improved electrode characteristics of olivine–$LiCoPO_4$ processed by high energy milling. *J. Power Sources* **2006**, *160*,523–528.
11. Yang, J.; Xu, J.J. Synthesis and characterization of carbon-coated lithium transition metal phosphates $LiMPO_4$ (M = Fe, Mn, Co, Ni) prepared via a nonaqueous sol-gel route. *J. Electrochem. Soc*. **2006**,*153*, A716–A723.
12. Piana, M.; Arrabito, M.; Bodoardo, S.; D'Epifanio, A.; Satolli, D.; Croce, F.; Scrosati, B. Characterization of phospho-olivines as materials for Li-ion cell cathodes. *Ionics* **2002**, *8*, 17–26.
13. Wang, D.; Wang, Z.; Huang, X.; Chen, L. Cracking causing cyclic instability of $LiFePO_4$ cathode material. *J. Power Sources* **2005**, *146*, 580–583.
14. Ruffo, R.; Mari, C.M.; Morazzoni, F.; Rosciano, F.; Scotti, R. Electrical and electrochemical behaviour of several $LiFe_xCo_{1-x}PO_4$ solid solutions as cathode materials for lithium ion batteries. *Ionics* **2007**, *13*, 287–291.
15. Wolfenstine, J.; Read, J.; Allen, J.L. Effect of carbon on the electronic conductivity and discharge capacity $LiCoPO_4$. *J. Power Sources* **2007**,*163*, 1070–1073.
16. Jang, I.C.; Son, C.G.; Yang, A.J.W.; Lee, S.M.G.; Cho, A.R.; Aravindan, V.; Park, G.J.; Kang, K.S.; Kim, W.S.; Cho, W.I.; *et al.* $LiFePO_4$ modified $Li_{1.02}(Co_{0.9}Fe_{0.1})_{0.98}PO_4$ cathodes with improved lithium storage properties. *J. Mater. Chem*. **2011**, *21*, 6510–6514.
17. Ju, H.; Wu, J.; Xu, Y. Lithium ion intercalation mechanism for $LiCoPO_4$ electrode. *Int. J. Energy Env. Eng.* **2013**, *4*, 22.
18. Yujuan, Z.; Suijun, W.; Chunsong, Z.; Dingguo, X. Synthesis and electrochemical performance of $LiCoPO_4$ micron-rods by dispersant-aided hydrothermal method for lithium ion batteries. *Rare Met.* **2009**, *28*, 117–121.

19. Huang, X.; Ma, J.; Wu, P.; Hu, Y.; Dai, J.; Zhu, Z.; Chen, H.; Wang, H. Hydrothermal synthesis of $LiCoPO_4$ cathode materials for rechargeable lithium ion batteries. *Mater. Lett.* **2005**, *59*, 578–582.
20. Kotobuki, M. Hydrothermal synthesis of carbon-coated $LiCoPO_4$ cathode material from various Co sources. *Int. J. Energy Env. Eng.* **2013**, *4*, 25.
21. Gangulibabu, D.; Bhuvaneswari, N.; Kalaiselvi, N.; Jayaprakash, P.; Periasamy, J. CAM sol–gel synthesized $LiMPO_4$ (M=Co, Ni) cathodes for rechargeable lithium batteries. *Sol–Gel Sci. Technol*. **2009**, *49*, 137–144.
22. Rajalakshmi, A.; Nithya, V.D.; Karthikeyan, K.; Sanjeeviraja, K.C.; Lee, Y.S.; Kalai Selvan, R. Physicochemical properties of V^{5+} doped $LiCoPO_4$ as cathode materials for Li-ion batteries. *J. Sol-Gel Sci. Technol.* **2013**, *65*, 399–410.
23. Sahnmukaraj, D.; Murugan, R. Synthesis and characterization of $LiNi_yCo_{1-y}PO4$ (y = 0–1) cathode materials for lithium secondary batteries. *Ionics* **2004**, *10*, 88–92.
24. Saint-Martin, R.; Franger, S. Growth of $LiCoPO_4$ single crystals using an optical floating-zone technique. *J. Cryst. Growth* **2008**, *310*, 861–864.
25. Xie, J.; Imanishi, N.; Zhang, T.; Hirano, A.; Takeda, Y.; Yamamoto, O. Li-ion diffusion kinetics in $LiCoPO_4$ thin films deposited on NASICON-type glass ceramic electrolytes by magnetron sputtering. *J. Power Sources* **2009**,*192*, 689–692.
26. Shui, J.L.; Yu, Y.; Yang, X.F.; Chen, C.H. $LiCoPO_4$-based ternary composite thin-film electrode for lithium secondary battery. *Electrochem. Commun.* **2006**, *8*, 1087–1091.
27. Li, H.H.; Jin, J.; Wei, J.P.; Zhou, Z.; Yan, J.J. Fast synthesis of core-shell $LiCoPO_4$/C nanocomposite via microwave heating and its electrochemical Li intercalation performances. *Electrochem. Commun*. **200**9, *11*, 95–98.
28. Doan, T.N.L.; Taniguchi, I. Cathode performance of $LiMnPO_4$/C nanocomposites prepared by a combination of spray pyrolysis and wet ball-milling followed by heat treatment. *J. Power Sources* **2011**,*196*, 1399–1408.
29. Devaraju, M.K.; Honma, I. Hydrothermal and solvothermal process towards development of $LiMPO_4$ (M = Fe, Mn) nanomaterials for lithium-ion batteries. *Adv. Energy Mater*. **2012**, *2*, 284–297.
30. Devaraju, M.K.; Sathish, M.; Honma, I. In *Handbook of Sustainable Engineering*; Kauffman, J., Lee, K.-M., Eds.; Springer: Dordrecht, The Netherlands, 2013; pp. 1149–1173.
31. Devaraju, M.K.; Rangappa, D.; Honma, I. Controlled synthesis of plate-like $LiCoPO_4$ nanoparticles via supercritical method and their electrode property. *Electrochem. Acta* **2012**, *85*, 548.
32. Hong, S.; Kim, S.J.; Chung, K.Y.; Chung, M.S.; Lee, B.G.; Kim, J. Continuous synthesis of lithium iron phosphate ($LiFePO_4$) nanoparticles in supercritical water: Effect of mixing tee. *J. Supercrit. Fluids* **2013**, *73*, 70–79.
33. Adschiri, T.; Lee, Y.W.; Goto, M.; Takamib, S. Green materials synthesis with supercritical water. *Green Chem.* **2011**, *13*, 1380–1390.
34. Hong, S.; Kim, S.J.; Chung, K.Y.; Lee, Y.W.; Kim, J.; Sang, B. Continuous synthesis of lithium iron phosphate nanoparticles in supercritical water: Effect of process parameters. *Chem. Eng. J.* **2013**, *229*, 313–323.

35. Nugroho, A.; Kim, S.J.; Kyung, W.C.; Chung, Y.; Kim, J. Facile synthesis of hierarchical mesoporous $Li_4Ti_5O_{12}$ microspheres in supercritical methanol. *J. Power Sources* **2013**, *244*, 164–169.
36. Nugroho, A.; Kim, S.J.; Chung, K.Y.; Kim, J. Synthesis of $Li_4Ti_5O_{12}$ in Supercritical water for Li-Ion batteries: Reaction mechanism and high-rate performance. *Electrochim. Acta* **2012**, *78*, 623–632.
37. Nugroho, A.; Chang, W.; Kim, S.J.; Chung, K.Y.; Kim, J. Superior high rate performance of core–shell $Li_4Ti_5O_{12}$/Carbon Nanocomposite synthesized by a supercritical alcohol approach. *RSC Adv.* **2012**, *2*, 10805–10808.
38. Jensen, K.; Christensen, M.; Tyrsted, C.; Brummerstedt Iversen, B. Real-time synchrotron powder X-ray diffraction study of the antisite defect formation during sub- and supercritical synthesis of $LiFePO_4$(4) and $LiFe_{1-x}Mn_x$ PO_4 nanoparticles. *J. Appl. Crystallogr.* **2011**, *44*, 287–294.
39. Rangappa, D.; Sone, K.; Kudo, T.; Honma, I. Directed growth of nanoarchitectured $LiFePO_4$ electrode by solvothermal synthesis and their cathode properties. *J. Power Sources* **2010**, *195*, 6167–6171.
40. Rangappa, D.; Sone, K.; Ichihara, M.; Kudo, T.; Honma, I. Rapid one-pot synthesis of $LiMPO_4$ (M = Fe, Mn) colloidal nanocrystals by supercritical ethanol process. *Chem. Commun.* **2010**, *46*, 7548.
41. Devaraju, M.K.; Dinesh, R.; Honma, I. Controlled synthesis of nanocrystalline Li_2MnSiO_4 particles for high capacity cathode application in lithium-ion batteries. *Chem. Commun.* **2012**, *48*, 2698–2700.
42. Dinesh, R.; Devaraju, M.K.; Tomai, T.; Unemoto, A.; Honma, I. Ultrathin nanosheets of Li_2MSiO_4 (M = Fe, Mn) as high-capacity Li-ion battery electrode. *Nano Lett.* **2012**, *12*, 1146.
43. Devaraju, M.K.; Tomai, T.; Unemoto, A.; Honma, I. Novel processing of lithium manganese silicate nanomaterials for Li-ion battery applications. *RSC Adv.* **2013**, *3*, 608–615.
44. Devaraju, M.K.; Tomai, T.; Honma, I. Supercritical hydrothermal synthesis of rod like Li_2FeSiO_4 particles for cathode application in lithium ion batteries. *Electrochem. Acta* **2013**, *109*, 75–78.
45. Devaraju, M.K.; Truong, Q.D.; Honma, I. Synthesis of Li_2CoSiO_4 nanoparticles and structure observation by annular bright and dark field electron microscopy. *RSC Adv.* **2013**, *43*, 20633–20638.
46. Devaraju, M.K.; Honma, I. One-pot synthesis of Li_2FePO_4F nanoparticles via a supercritical fluid process and characterization for application in lithium-ion batteries. *RSC Adv.* **2013**, *43*, 19849–19852.
47. Liu, J.; Conry, T.E.; Song, X.Y.; Yang, L.; Doeff, M.M.; Richardson, T.J. Spherical nanoporous $LiCoPO_4$/C composites as high performance cathode materials for rechargeable lithium-ion batteries. *J. Mater. Chem.* **2011**, *21*, 9984–9987.
48. Doan, T.N.L.; Taniguchi, I. Preparation of $LiCoPO_4$/C nanocomposite cathode of lithium batteries with high rate performance. *J. Power Sources* **2011**, *196*, 5679–5684.
49. Truong, Q.D.; Devaraju, M.K.; Tomai, T.; Honma, I. Direct observation of antisite defects in $LiCoPO_4$ cathode materials by annular dark and bright field electron microscopy. *ACS Appl. Mater. Interfaces* **2013**, *5*, 9926–9932.

50. Han, D.W.; Kang, Y.M.; Yin, R.Z.; Song, M.S.; Kwon, H.S. Effects of Fe doping onthe electrochemical performance of $LiCoPO_4$/C composites for high power-density cathode materials. *Eletrochem. Commun.* **2009**, *11*, 137–140.
51. Ehrenberg, H.; Bramnik, N.N.; Senyshyn, A.; Fuess, H. Crystal and magnetic structures of electrochemically delithiated $Li_{1-x}CoPO_4$ phases. *Solid State Sci.* **2009**, *11*, 18–23
52. Bramnik, N.N.; Nikolowski, K.; Baehtz, C.; Bramnik, K.G.; Ehrenberg, H. Phase transitions occurring upon lithium insertion−extraction of $LiCoPO_4$. *Chem. Mater.* **2007**, *19*, 908–915.
53. Izumi, F.; Ikeda, T. A Rietvled-analysis program REITAN-98 and its applications to zeolites. *Mater. Sci. Forum* **2000**, *321–324*, 198–203.